Glycolaldehyde + OH gas phase reaction: A quantum chemistry + CVT/SCT approach

ARTICLE *in* THE JOURNAL OF PHYSICAL CHEMISTRY A · FEBRUARY 2005

Impact Factor: 2.69 · DOI: 10.1021/jp047490s · Source: PubMed

4 AUTHORS, INCLUDING:

Annia Galano
Metropolitan Autonomous University
153 PUBLICATIONS **3,371** CITATIONS
SEE PROFILE

Juan Raul Alvarez-Idaboy
Universidad Nacional Autónoma de México
121 PUBLICATIONS **2,177** CITATIONS
SEE PROFILE

Glycolaldehyde + OH Gas Phase Reaction: A Quantum Chemistry + CVT/SCT Approach

Annia Galano,*,† J. Raúl Alvarez-Idaboy,*,† Ma. Esther Ruiz-Santoyo,† and Annik Vivier-Bunge‡

Instituto Mexicano del Petróleo, Eje Central Lázaro Cárdenas 152, 007730 México D. F., México, and Universidad Autónoma Metropolitana, Iztapalapa, 09340 México D. F., México

Received: June 10, 2004; In Final Form: October 20, 2004

We present a theoretical study of the mechanism and kinetics of the OH hydrogen abstraction from glycolaldehyde. Optimum geometries, frequencies, and gradients have been computed at the BHandHLYP/6-311++G(d,p) level of theory for all stationary points, as well as for additional points along the minimum energy path (MEP). Energies are obtained by single-point calculations at the above geometries using CCSD(T)/6-311++G(d,p) to produce the potential energy surface. The rate coefficients are calculated for the temperature range 200−500 K by using canonical variational theory (CVT) with small-curvature tunneling (SCT) corrections. Our analysis suggests a stepwise mechanism involving the formation of a reactant complex in the entrance channel and a product complex in the exit channel, for all the modeled paths. The overall agreement between the calculated and experimental kinetic data that are available at 298 K is very good. This agreement supports the reliability of the parameters obtained for the temperature dependence of the glycolaldehyde + OH reaction. The expressions that best describe the studied reaction are $k_{overall} = 7.76 \times 10^{-13}\, e^{1328/RT}$ cm^3·molecule^{-1}·s^{-1} and $k_{overall} = 1.09 \times 10^{-21} T^{3.03}\, e^{3187/RT}$ cm^3 molecule^{-1} s^{-1}, for the Arrhenius and Kooij approaches, respectively. The predicted activation energy is (−1.36 ± 0.03) kcal/mol, at about 298 K. The agreement between the calculated and experimental branching ratios is better than 10%. The intramolecular hydrogen bond in OO-*s*-cis glycolaldehyde is found to be responsible for the discrepancies between SAR and experimental rate coefficients.

Introduction

Glycolaldehyde (hydroxyethanal, hydroxyacetaldehyde) is the simplest hydroxycarbonyl and a significant compound in atmospheric chemistry. It can be directly emitted by biomass fires[1−5] or formed in oxidation reactions of volatile organic compounds (VOCs).[6−13] During daytime, the main loss processes of glycolaldehyde in the troposphere are photolysis and reaction with OH radicals. However, to the best of our knowledge, only two articles have been published concerning its reaction with OH.[14,15] Kwok and Atkinson[16] have listed glycolaldehyde as one of the molecules for which the measured rate coefficient differs, by more than a factor of 2, from the one estimated using structure−activity relationships (SAR).

Niki et al.[14] determined the relative rate constant of the OH radical toward glycolaldehyde, using acetaldehyde as reference and the FTIR spectroscopic method. They reported a rate constant of (1.0 ± 0.2) × 10^{-11} cm^3 molecule^{-1} s^{-1} for the overall reaction. The authors also reported that the glycolaldehyde + OH reaction has two main channels: hydrogen abstraction from either −CHO or −CH$_2$, with contributions of 80% and 20%, respectively. More recently, Bacher et al.[15] used the same technique with propene and acetaldehyde as references and obtained a rate constant of (1.1 ± 0.3) × 10^{-11} cm^3 molecule^{-1} s^{-1}, in excellent agreement with the value previously reported by Niki et al.[14] The authors also found that the glycolaldehyde loss by reaction with OH probably exceeds the one due to photolysis. In both articles[14,15] the rate constant was measured only at 298 K. Therefore, the Arrhenius parameters were not reported.

In the current work, the glycolaldehyde + OH reaction has been modeled based on the experimental[17−20] and theoretical finding[21−24] that OH reacts with aldehydes by H abstraction rather than by addition to the carbonyl group, as well as on the results from ref 14, as discussed above. Accordingly, only hydrogen abstraction paths have been considered. Each path has been modeled taking into account the formation of the corresponding reactant complex, as proposed in theoretical studies[24−30] of OH radicals reactions with oxygenated compounds. The role of reactant complexes in bimolecular reactions has been recently reviewed.[31] These intermediates have also been studied experimentally.[32,33] Moreover, it has been established that the presence of an attractive well at the entrance channel of a potential energy surface can influence the dynamics and hence the course of the reaction.[31] The existence of a reactant complex is to be expected when there is an attractive encounter between reactants, and it may manifest itself in terms of negative temperature dependence. The role of such complexes has been recently pointed out for the OH reaction with acetone and acetaldehyde,[34] which show curved Arrhenius plots and negative temperature dependences.

In addition a conformational study of glycolaldehyde has been performed, and the relative population of the most stable conformers has been taken into account in the overall rate constant calculation.

The aim of this work is to determine Arrhenius parameters for the OH radical reaction with glycolaldehyde, by assuming that it occurs according to a complex mechanism that involves

* Corresponding authors. E-mail: A.G., agalano@imp.mx; J.R.A.-I., jidaboy@imp.mx

† Instituto Mexicano del Petróleo.

‡ Universidad Autónoma Metropolitana.

10.1021/jp047490s CCC: $30.25
Published on Web 12/13/2004

a barrier-less first step that leads to the formation of a thermally stabilized reactant complex. In the second step, an energy barrier that is higher than the apparent activation energy leads to the formation of a product complex, and then to the corresponding radical and water. A description of the temperature dependence for the glycolaldehyde + OH reaction is given.

The data reported here are relevant to the understanding of the tropospheric chemistry of glycolaldehyde and to the assessment of its importance as a secondary pollutant.

Computational Details

Five stationary points have been modeled along each reaction path: the isolated reactants, the reactant complex, the transition state, the product complex, and the products. Full geometry optimizations were performed with the Gaussian 98[35] program using the BHandHLYP hybrid HF-density functional[36,37] and the 6-311++G(d,p) basis set. The energies of all the stationary points were improved by single point calculations at the CCSD-(T)/6-311++G(d,p) level of theory. Unrestricted calculations were used for open shell systems. Frequency calculations were carried out for all the stationary points at the DFT level of theory and local minima and transition states were identified by the number of imaginary frequencies (NIMAG = 0 or 1, respectively). Zero point energies (ZPE) and thermal corrections to the energy (TCE) at 298.15 K were included in the determination of the activation energies and of the heats of reaction, respectively.

Rate coefficients were calculated using the canonical variational theory (CVT)[38−44] and small-curvature tunneling (SCT)[41−47] corrections, implemented in the cseo.net web site.[48] The minimum-energy paths (MEP)[49,50] were calculated by the intrinsic reaction coordinate (IRC) method[51,52] at the BHandHLYP/6-311G++(d,p) level of theory, using mass-scaled Cartesian coordinates[53,54] with a reduced mass, μ, equal to 1 amu. Two hundred points were modeled on either side of the saddle points, with a gradient step size of 0.01 bohr. Force constants, harmonic vibrational frequencies and normal-mode vectors for the $3N - 7$ degrees of freedom that are orthogonal to the reaction path were computed at selected points along the IRC.

The canonical variational theory (CVT)[38−44] is an extension of the transition state theory (TST).[55,56] This theory minimizes the errors due to recrossing trajectories[57−59] by moving the dividing surface along the MEP so as to minimize the rate. The reaction coordinate (s) is defined as the distance along the MEP, with the origin located at the saddle point and is negative on the reactants side and positive on the products side of the MEP. For a canonical ensemble at a given temperature T, the canonical variational theory (CVT) thermal rate constant is given by

$$k^{\mathrm{CVT}}(T,s) = \min\{k^{\mathrm{GT}}(T,s)\} \tag{1}$$

where $k^{\mathrm{GT}}(T,s)$ is the rate constant for the passage through the generalized transition state (GT)[60−64] that intersects the MEP at s:

$$k^{\mathrm{GT}}(T,s) = \sigma(s)\frac{k_{\mathrm{B}}T}{h}\frac{Q^{\mathrm{GT}}(T,s)}{Q^{\mathrm{R}}(T)}\exp\left[-\frac{V_{\mathrm{MEP}}(s)}{k_{\mathrm{B}}T}\right] \tag{2}$$

In this expression, k_{B} and h are the Boltzmann and Planck constants, T is temperature, Q^{GT} and Q^{R} are the partition functions per unit volume of the generalized transition state and of the reactants, and $V_{\mathrm{MEP}}(s)$ is the potential energy of the MEP at s.

Accurate rate constant calculations require the correct computation of the partition functions (Q). In this work, the hindered rotor approximation has been used to correct the Qs corresponding to internal rotations with torsional barriers comparable to RT. Direct inspection of the low-frequency modes of the studied stationary points indicates that there are several modes that correspond to hindered rotations. These modes should be treated as hindered rotors instead of vibrations.[65] To make this correction, these modes were removed from the vibrational partition function of the corresponding species and replaced by the hindered rotor partition function (Q^{HR}).

In our calculations we have adopted the analytical approximation to Q^{HR} for a one-dimensional hindered internal rotation proposed by Ayala and Schlegel:[66]

$$Q^{\mathrm{HR}}(T) = \left(\frac{Q_i^{\mathrm{h.o.q}}}{Q_i^{\mathrm{h.o.cl}}}\right)Q_i^{\mathrm{FR}}\frac{\left(1 + P_2\exp\left[-\frac{V_0}{2k_{\mathrm{B}}T}\right]\right)}{\left(1 + P_1\exp\left[-\frac{V_0}{2k_{\mathrm{B}}T}\right]\right)}\exp\left[-\frac{V_0}{2k_{\mathrm{B}}T}\right]J_0\left(\frac{iV_0}{2k_{\mathrm{B}}T}\right) \tag{3}$$

where Q_i^{FR} is the free-rotor partition function, P_1 and P_2 are polynomial functions of $1/Q_i^{\mathrm{FR}}$, J_0 is Bessel's function, T is the temperature, and k_{B} is Boltzmann's constant. The internal rotational barrier, V_0, was calculated from the rotational potential curve computed at BHandHLYP/6-311++G(d,p) level using the relaxed scan with 72 points and 5° steps. The quantum and classical partition functions $Q_i^{\mathrm{h.o.q}}$ and $Q_i^{\mathrm{h.o.cl}}$ are defined as

$$Q_i^{\mathrm{h.o.q}} = \frac{\mathrm{e}^{-u/2}}{1 - \mathrm{e}^{-u}} \tag{4}$$

and

$$Q_i^{\mathrm{h.o.cl}} = \frac{1}{u} \tag{5}$$

with

$$u = \frac{h\nu_i}{k_{\mathrm{B}}T} \tag{6}$$

where h is Planck's constant and ν_i is the vibrational frequency associated with the hindered rotation. Following the recommendation in ref 66, the free rotor partition function has been calculated as

$$Q_i^{\mathrm{FR}}(T) = \left(\frac{8\pi^3 k_{\mathrm{B}}}{h^2{\sigma_{\mathrm{int}}}^2}\right)^{1/2}(I'T)^{1/2} \tag{7}$$

where I' is the reduced moment of inertia for the internal rotation and σ_{int} is the periodicity of the internal rotation potential. The σ_{int} values are considered equal to the number of minima or maxima in the torsional potential energy curve. The reduced moments of inertia were calculated as

$$I = \frac{I_{\mathrm{top1}}I_{\mathrm{top2}}}{I_{\mathrm{top1}} + I_{\mathrm{top2}}} \tag{8}$$

where the moment of inertia of the rotating fragments (I_{top}) about the axis of internal rotation was calculated as $I_{\mathrm{top}} = \Sigma\, m_i r_i^2$ with m_i = atomic mass of atom i and r_i = distance of atom i

from the rotation axis, and the sum runs over all atoms in the rotating fragment.

The reaction path symmetry factor, $\sigma(s)$ accounts for the number of equivalent reaction paths. In this work, it is calculated according to the general expression derived by Pechukas et al.[67]

$$\sigma(s) = \frac{n\sigma^{R}}{\sigma^{GT}(s)} \tag{9}$$

where n is the number of identical transition states, σ^{R} is the product of the usual rotational symmetry numbers of both reactants, and $\sigma^{GT}(s)$ is the symmetry number for the generalized transition state at s. In this work, σ^{GT} was considered independent of s, thus $\sigma(s)$ becomes a constant, σ.

The quantum mechanical effect on the motion along the reaction coordinate is included in the kinetics calculations by multiplying the CVT rate constant by a temperature-dependent transmission coefficient $\kappa(T)$. Therefore, the final expression for the rate constant is given by

$$\kappa(T) = \kappa(T)k^{CVT}(T,s) \tag{10}$$

where $\kappa(T)$ may be computed using the small-curvature (SCT) method,[41−47] which constitutes a generalization of the Marcus−Coltrin method.[68] In SCT it is assumed that the tunneling path is displaced from the MEP to a concave-side vibrational turning point in the direction of the internal centrifugal force. In this method, the probability that a system with energy E be transmitted through the ground-state level of the transition state is approximated by the centrifugal-dominant−small-curvature semiclassical adiabatic ground-state method (CD−SCSAG).[69,70] The SCT transmission coefficient includes the effect of the reaction path curvature on the transmission probability, $P(E)$, which is calculated as

$$P(E) = 1/\{1 + \exp[2\theta(E)]\} \tag{11}$$

where $\theta(E)$ is the imaginary action integral evaluated along the tunneling path:

$$\theta(E) = \frac{2\pi}{h}\int_{S_1}^{S_2} \sqrt{2\mu_{eff}(s)|E - V_a^{G}(s)|}\, ds \tag{12}$$

The integration limits S_1 and S_2 are the reaction coordinate classical turning points; μ_{eff} is the reduced mass, which introduces the reaction path curvature; and $V_a^{G}(s)$ is the adiabatic ground-state potential.

The SCT approach provides the most accurate treatment of tunneling for the amount of data of the MEP determined in this study. Methods for large curvature cases[46] require more information and were considered to be unnecessary, considering the fact that the SCT method has been successfully used in the study of several OH abstraction reactions.[71−77]

Results and Discussion

Geometries. Glycolaldehyde has two internal rotational degrees of freedom: the central C−C bond torsion and the C−O hydroxyl torsion. The corresponding variables ϕ_1 and ϕ_2 can be identified with the O3C2C1O4 and C2C1O4H8 dihedral angles (Figure 1). Several different minima were fully optimized at BHandHLYP/6-311++G(d,p) level of calculation and the two most stable conformations will be the only ones considered in this work. They correspond to the OO-*s*-cis and OO-*s*-trans isomers and their contribution to the total population is 94% and 6%, respectively, at 298 K. Structure **I** (Figure 1) is stabilized by an intramolecular hydrogen bond between the carbonyl oxygen and the hydroxyl hydrogen at 2.130 Å. This interaction has been previously described by Ratajczyk et al.[78] and by Senent[79] at MP2/aug-cc-pDTZ and MP4(SDTQ)/cc-pVQZ levels of calculations, respectively. The adiabatic barriers corresponding to the cis → trans conversion were found to be equal to 5.4 + 0.4 kcal/mol, at BHandHLYP/6-311++G(d,p) level of theory, in perfect agreement with the values reported by Senent[79] (5.4 + 0.5 kcal/mol). These two values correspond to rotation around the C1−C2 bond followed by rotation around the C1−O4 bond, both motions are necessary to go from conformer **I** to conformer **II** (see ref 79 for more details).

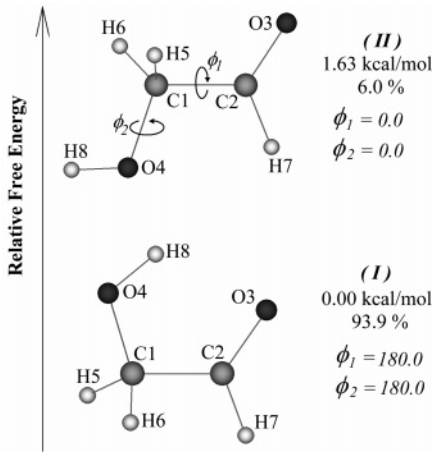

Figure 1. Fully optimized BHandHLYP/6-311++G(d,p) glycolaldehyde conformers.

Three reaction channels have been modeled for both conformers, **I** and **II**:

$$HOCH_2CHO + OH \rightarrow HOCH_2CO + H_2O \quad (a)$$

$$\rightarrow HOCHCHO + H_2O \quad (b)$$

$$\rightarrow OCH_2CHO + H_2O \quad (c)$$

Each of them consists of three steps, namely: (1) the formation of a reactant complex from the isolated reactants, (2) the formation of a product complex from the reactant complex, and (3) the formation of a radical and water from the product complex:

$$G + OH \underset{k_{-1}}{\overset{k_1}{\rightleftharpoons}} RC \xrightarrow{k_2} PC \underset{k_{-1}}{\overset{k_3}{\rightleftharpoons}} R + H_2O$$

where G represents glycolaldehyde, and RC, PC, and R represent the reactant complex, product complex and radical product corresponding to each particular path.

In all, six reactant complexes were identified (Figure 2). The reactant complex corresponding to abstraction from the −CHO group in conformer **I** (**RC-Ia**) is stabilized by the attractive interaction between H in the OH radical and the O atom in the carbonyl group of glycolaldehyde, at a distance (d) of 1.929 Å. This complex shows $C_s(^2A')$ or σ symmetry, the unpaired electron being located in an orbital in the molecular plane. A Bader topological analysis[80] of the BHandHLYP/6-311++G-(d,p) wave function was performed in order to characterize this interaction. The electronic charge density (ρ) and the Laplacian of ρ at the bond critical point were found to be $\rho_{3-10} = 0.0247$ and $\nabla^2\rho_{3-10} = -0.0238$, respectively. The atom numbering used in this work corresponds to that in Figure 1, and the O and H atoms in the OH radical are referred to as 9 and 10, respectively. The reactant complex corresponding to abstraction from $-CH_2$ in conformer **I** (**RC-Ib**) is caused by the attractive

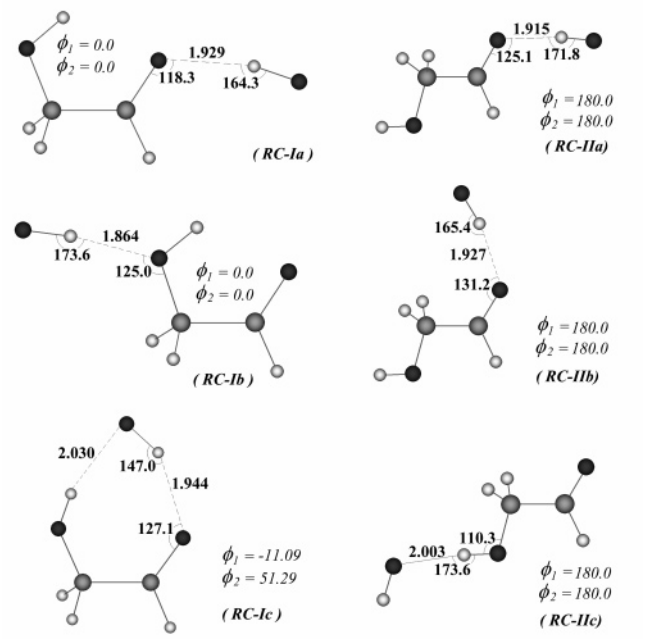

Figure 2. Fully optimized BHandHLYP/6-311++G(d,p) reactant complexes of the glycolaldehyde + OH reaction.

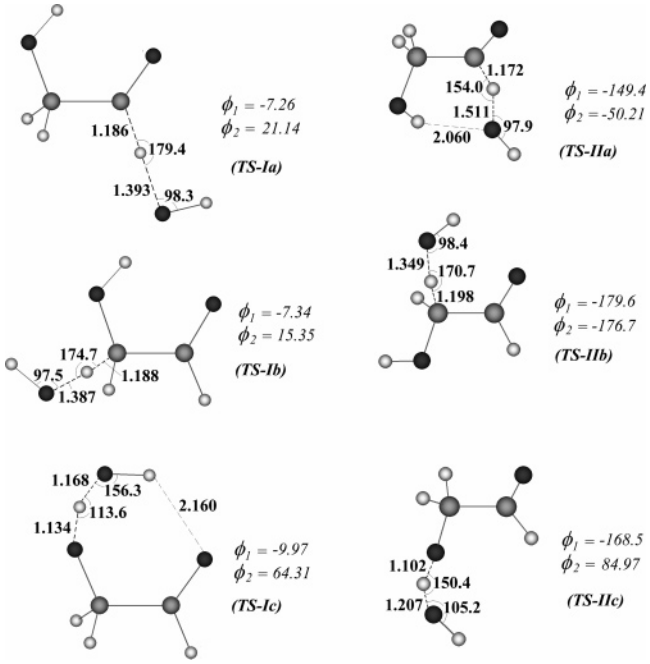

Figure 3. Fully optimized BHandHLYP/6-311++G(d,p) transition states of the glycolaldehyde + OH reaction.

interaction between H in the OH radical and the O atom in the hydroxyl group, at a distance $d_{4-10} = 1.864$ Å. This complex also shows $C_s(^2A')$ symmetry and its Bader topological analysis gives the following values for the bond critical point: $\rho_{4-10} = 0.0274$ and $\nabla^2\rho_{4-10} = -0.0282$. Two attractive interactions are responsible for the formation of the RC corresponding to abstraction from −OH in conformer **I** (**RC-Ic**). The main one occurs between the H atom in the OH radical and the O in the carbonyl group, with $d_{3-10} = 1.944$ Å, $\rho_{3-10} = 0.0244$, and $\nabla^2\rho_{3-10} = -0.0234$. The other one, between O in the OH radical and H in the hydroxyl group has $d_{8-9} = 2.030$ Å, $\rho_{8-9} = 0.0204$, and $\nabla^2\rho_{8-9} = -0.0188$. The presence of these interactions causes the reactant complex to form a ringlike structure that is characterized by a ring critical point, with $\rho = 0.0082$ and $\nabla^2\rho = -0.0087$.

The three reactant complexes for conformer **II** (Figure 2) will be described next. All of them show $C_s(^2A')$ symmetry, with the unpaired electron located in an orbital in the molecular plane. **RC-IIa**, which corresponds to hydrogen abstraction from the aldehydic group, is formed due to the interaction between the H atom in the OH radical and the O atom in the carbonyl group, at a distance $d_{3-10} = 1.915$ Å. The Bader topological analysis gives the following values for the bond critical point: $\rho_{3-10} = 0.0249$ and $\nabla^2\rho_{3-10} = -0.0245$. The RC corresponding to H abstraction from the $-CH_2$ group (**RC-IIb**) is caused by the same interaction as in **RC-IIa**, with $d_{3-10} = 1.927$ Å, $\rho_{3-10} = 0.0241$, and $\nabla^2\rho_{3-10} = -0.0238$. **RC-IIc** (Figure 2) corresponds to H abstraction from the hydroxyl group in conformer **II** and is caused by the interaction between O in the OH radical and H in the hydroxyl group. This RC shows $d_{8-9} = 2.003$ Å, $\rho_{8-9} = 0.0201$, and $\nabla^2\rho_{8-9} = -0.0203$.

All the transition state (TS) structures considered in this work are shown in Figure 3. The BHandHLYP/6-311++G(d,p) fully optimized transition structures show no symmetry. The main structural change associated with the formation of the aldehydic abstraction TS (**TS-Ia**) is an elongation of d_{2-7} by 0.088 Å, compared to free glycolaldehyde. Other minor variations observed in **TS-Ia** with respect to reactants are the shortening of the C2O3 bond by 0.013 Å and the elongation of the C1C2 bond by 0.005 Å. The attack of the OH radical is found to be collinear, with the C2H7O9 angle equal to 179.4°. **TS-Ib** in Figure 3 corresponds to abstraction from the $-CH_2$ group in conformer **I**. It shows an elongation of 0.097 Å compared to the free reactant, and slight shortening of distances d_{1-4} and d_{1-2}, by 0.022 and 0.005 Å, respectively. The OH attack is found to be almost collinear, with a C1H5O9 angle of 174.7°. The transition state corresponding to channel **c** in conformer **I** (**TS-Ic**) shows an elongation of 0.178 Å in the O4H8 bond and a shortening of 0.012 Å in the C1O4 bond. A stabilizing intramolecular hydrogen bond is found between H in the OH fragment and the carbonylic O in the glycolaldehyde fragment, with $d_{3-10} = 2.160$ Å. This interaction has been characterized by Bader's topological analysis, and two critical points were found, a bond critical point with $\rho_{3-10} = 0.0168$ and $\nabla^2\rho_{3-10} = -0.0153$ and a ring critical point with $\rho = 0.0098$ and $\nabla^2\rho = -0.0116$.

The TSs corresponding to abstraction from −CHO (**TS-IIa**), $-CH_2$ (**TS-IIb**), and −OH (**TS-IIc**) groups in conformer **II** are also shown in Figure 3. The main structural change associated with the formation of **TS-IIa** is the elongation of d_{2-7} by 0.073 Å, compared to free glycolaldehyde. Other minor variations observed in **TS-IIa** with respect to the reactant are the shortening of the C2O3 bond by 0.015 Å and the elongation of the C1C2 bond by 0.011 Å. The attack of the OH radical is found to be less collinear, the C2H7O9 angle being equal to 154.0°. **TS-IIa** shows a ringlike structure that is caused by an intramolecular interaction between O in the OH radical and H in the hydroxyl group, with $d_{8-9} = 2.060$ Å. It has been characterized by Bader's topological analysis and two critical points were found, a bond critical point with $\rho_{8-9} = 0.0204$ and $\nabla^2\rho_{8-9} = -0.0188$ and a ring critical point with $\rho = 0.0131$ and $\nabla^2\rho = -0.0158$. **TS-IIb** shows a C1H5 bond elongation of 0.109 Å compared to the free reactant, and slight shortenings of 0.027 and 0.010for distances d_{1-4} and d_{1-2}, respectively. The OH attack was found to be almost collinear, with a C1H5O9 angle of 170.7°. **TS-IIc** shows an elongation of 0.153 Å in the O4H8 bond and a shortening of 0.012 Å in the C1O4 bond.

The six product complexes (PC) corresponding to all the computed paths have been also modeled and fully optimized

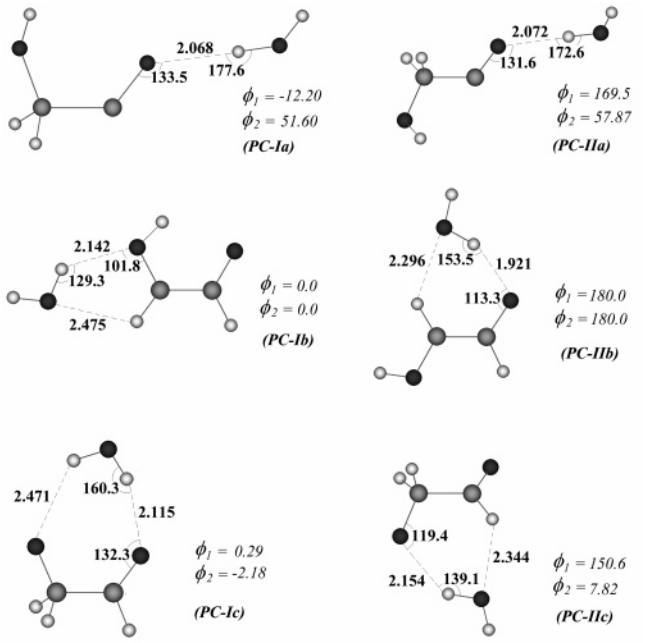

Figure 4. Fully optimized BHandHLYP/6-311++G(d,p) product complexes of the glycolaldehyde + OH reaction.

(Figure 4). The product complex corresponding to the abstraction from the −CHO group in conformer **I** (**PC-Ia**) is formed due to the attractive interaction between an H in the water molecule and the O atom in the carbonyl group of the forming radical, at an interaction distance of 2.068 Å. This complex shows no symmetry. A Bader topological analysis of its BHandHLYP/6-311++G(d,p) wave function was performed and a bond critical point was found, with $\rho_{3-7} = 0.0159$ and $\nabla^2\rho_{3-7} = -0.0171$. The product complex corresponding to abstraction from $-CH_2$ in conformer **I** (**PC-Ib**) is caused by two attractive interactions. One of them occurs between H in the water molecule and the O atom in the hydroxyl group of the forming radical, with $d_{4-5} = 2.142$ Å. The other interaction occurs between O in the water molecule and H in the −CH group in the forming radical. This complex shows $C_s(^2A')$ symmetry, and its Bader topological analysis gives the following values for the bond critical points, $\rho_{4-5} = 0.0148$, $\nabla^2\rho_{4-5} = -0.0162$, $\rho_{6-9} = 0.0085$, $\nabla^2\rho_{6-9} = -0.0090$. The presence of these interactions causes a ringlike structure of the PC, which is characterized by a ring critical point with $\rho = 0.0076$ and $\nabla^2\rho = -0.0105$. The formation of the PC corresponding to abstraction from the −OH in conformer **I** (**PC-Ic**) is also caused by two attractive interactions. The main one occurs between one H atom in the water molecule and the O in the carbonyl group, with $d_{3-10} = 2.115$ Å, $\rho_{3-10} = 0.0157$, and $\nabla^2\rho_{3-10} = -0.01544$. The other one, between the H and the O atoms in the former hydroxyl group, has $d_{4-8} = 2.471$ Å, $\rho_{4-8} = 0.0087$, and $\nabla^2\rho_{4-8} = -0.0077$. The ringlike structure of this PC is characterized by a ring critical point with $\rho = 0.0052$ and $\nabla^2\rho = -0.0056$.

The product complexes corresponding to H abstractions from conformer **II** are also shown in Figure 4. **PC-IIa**, which corresponds to hydrogen abstraction from the aldehydic group, is formed due to the interaction between one H atom in the water molecule and the O atom in the carbonyl group, with $d_{3-7} = 2.072$ Å. This complex shows no symmetry. Its Bader topological analysis gives the following values for the bond critical point: $\rho_{3-7} = 0.0156$ and $\nabla^2\rho_{3-7} = -0.0168$. The PC corresponding to the H abstraction from the $-CH_2$ group (**PC-IIb**) has $C_s(^2A')$ symmetry and a ringlike structure caused by two attractive interactions. One of them occurs between one H in the water molecule and the O atom in the carbonyl group of the forming radical, with $d_{3-5} = 1.921$ Å, $\rho_{3-59} = 0.0257$, and $\nabla^2\rho_{3-5} = -0.0245$. The other one is between the O in the water molecule and the H in the −CH group of the forming radical, with $d_{6-9} = 2.296$ Å, $\rho_{6-9} = 0.0114$, and $\nabla^2\rho_{6-9} = -0.0118$. The corresponding ring critical point is characterized by $\rho = 0.0073$ and $\nabla^2\rho = -0.0094$. **PC-IIc** (Figure 4) presents no symmetry and corresponds to the H abstraction from the hydroxyl group in conformer **II**. It also shows a ringlike structure caused by two interactions, one between the H and the O atoms in the former hydroxyl group, with $d_{4-8} = 2.154$ Å, $\rho_{4-8} = 0.0157$, and $\nabla^2\rho_{4-8} = -0.0149$; and the other between the O in the water molecule and H in the −CHO group of the radical, with $d_{7-9} = 2.344$ Å, $\rho_{7-9} = 0.0121$, and $\nabla^2\rho_{7-9} = -0.0103$. The ring critical point has $\rho = 0.0064$ and $\nabla^2\rho = -0.0071$.

The radical products corresponding to all abstraction paths from both conformers are shown in Figure 5. Those corresponding to abstractions from $-CH_2$ and OH groups (**R-Ib**, **R-IIb**, **R-Ic**, and **R-IIc**) present $C_s(^2A')$ or σ symmetry, with the unpaired electron located in an orbital in the molecular plane. Those corresponding to abstractions from the −CHO group (**R-Ia** and **R-IIa**) show no symmetry. Their geometries remain nearly unchanged, compared to those of the corresponding product complexes.

TABLE 1: CCSD(T)//BHandHLYP/6-311++G(d,p) Energies, in kcal/mol, Relative to the Isolated Reactants

conformer I		conformer II	
RC-Ia[a]	−3.4	**RC-IIa**[a]	−3.7
RC-Ib[a]	−4.6	**RC-IIb**[a]	−3.6
RC-Ic[a]	−3.8	**RC-IIc**[a]	−3.5
TS-Ia[a]	−1.1	**TS-IIa**[a]	−2.4
TS-Ib[a]	−0.1	**TS-IIb**[a]	0.2
TS-Ic[a]	4.6	**TS-IIc**[a]	3.7
PC-Ia[b]	−26.6	**PC-IIa**[b]	−28.5
PC-Ib[b]	−36.9	**PC-IIb**[b]	−36.6
PC-Ic[b]	−10.4	**PC-IIc**[b]	−14.0
R-Ia + H_2O[b]	−25.4	**R-IIa** + H_2O[b]	−27.4
R-Ib + H_2O[b]	−34.5	**R-IIb** + H_2O[b]	−31.1
R-Ic + H_2O[b]	−7.3	**R-IIc** + H_2O[b]	−7.7

[a] Including ZPE corrections. [b] Including TCE corrections at 298 K.

Energies. The energies of all the modeled stationary points, relative to the isolated reactants, are shown in Table 1. They show that all the studied stationary points are lower in energy than the corresponding reactants, with the exception of the transition states for H abstraction from the hydroxyl group in both conformers and from the $-CH_2$ group in conformer **II**. Therefore, negative overall energy barriers ($E_{overall} = E_{TS} - \Sigma E_{reactants}$) are observed for the aldehydic abstractions and for the abstraction from the $-CH_2$ group in the main conformer. These energy barriers were calculated before the energetic shift. The presence of a reactant complex explains the $E_{overall}$ negative sign and the complex mechanism proposed leads to the following adiabatic effective barriers ($E_{eff} = E_{TS} - E_{RC}$): E_{eff}(**Ia**) = 2.3, E_{eff}(**Ib**) = 4.6, E_{eff}(**Ic**) = 8.3, E_{eff}(**IIa**) = 1.4, E_{eff}(**IIb**) = 3.8, and E_{eff}(**IIc**) = 7.2 kcal/mol. These values show that, for both conformers, aldehydic abstractions present the lowest effective barriers, while abstraction from the OH sites are the least favored paths. The stabilization energies of the reactant complexes ($E_{RC} - E_{React}$) for all the modeled abstractions are larger than 3 kcal/mol, which supports the complex mechanism assumption.

Intrinsic reaction coordinate calculations (IRC) have been performed at the BHandHLYP/6-311++G(d,p) level of theory in order to obtain the minimum energy paths (MEP). The

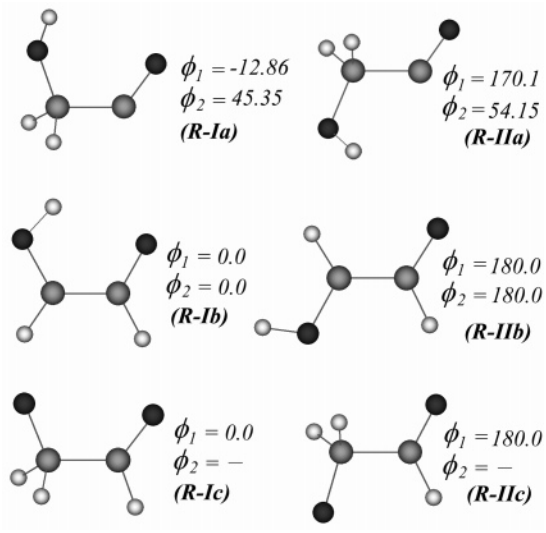

Figure 5. Fully optimized BHandHLYP/6-311++G(d,p) radical products of the glycolaldehyde + OH reaction.

calculations were carried out starting from the fully optimized saddle-point geometries, and then moving downhill along the reactant and product channels, in mass-weighted Cartesian coordinates. One hundred points were calculated in each direction at an even gradient step size of 0.01 bohr. The reaction coordinate s is defined as the signed distance from the saddle point, with $s < 0$ referring to the reactants side and $s > 0$ to the products side. As a reasonable compromise between speed and accuracy, and based on the curvature of the surface, 12 points, six on each side of the saddle point, were chosen to construct the MEP. They were chosen using the automated method provided in TheRate software.[81] According to the authors six to ten points are typically sufficient to properly describe the MEP. For all the chosen points, energies were then improved by single point calculations at the CCSD(T)/6-311++G(d,p) level of theory, and they were used in conjunction with gradients and frequencies computed at the BHandHLYP/6-311++G(d,p) level.

Figure 6 presents the ground state vibrationally adiabatic potential energy paths for the aldehydic abstractions from both conformers, according to

$$V_a^G(s) = V_{MEP}(s) + E_{int}(s) \quad (13)$$

where $V_{MEP}(s)$ is the classical potential energy path (the CCSD(T) electronic profile) and $E_{int}(s)$ is the local zero-point energy (ZPE) at s.

An attempt to extend the calculation of the MEPs to reach the reactant complexes directly was unsuccessful. However, in all the studied cases, when an optimization to minima is performed on the last optimized point on the IRC, it converges to the corresponding RC. Nevertheless, this should not compromise the reliability of our results since the CVT calculations extrapolate the MEP to the reactant and products stationary points, so the curve and its first derivative are continuous at the connecting points.[81]

In Figure 6, all the potential surfaces were obtained by cubic spline interpolations on the corresponding energies of the selected points mentioned above. The electronic curve (V_{MEP}) is represented twice. The dashed line is the electronic energy obtained using the CCSD(T) single point calculations at the BHandHLYP geometries. This procedure for the calculation of the MEP has become common in the study of polyatomic systems because it is relatively inexpensive from a computational point of view and it usually reproduces correctly the main features of the reaction path. It is known as B//A, and it consists of geometry optimizations at a given level (A) followed by single point calculations, without optimization, at a higher level (B). The V_{MEP} obtained using this technique presents a maximum that is shifted toward the reactants valley by about −0.2 bohr with respect to the maximum at the A level of calculation. Espinosa-Garcia and Corchado[82] argue that, when the MEP is constructed using the B//A technique, the energy maximum is artificially located away from the saddle point corresponding to the level of optimization (A). This shift, that is simply a numerical effect, could be mistaken with a variational effect and mislead the kinetic calculations. Consequently, we have used the modification proposed by Espinosa-Garcia and Corchado,[82] which consists of simply moving the maximum of the single-point calculation curve, B//A, to its original position ($s = 0$) at the A//A level. The corresponding curves for V_{MEP} are shown as solid lines in Figure 6. It should be noticed that according to this procedure the frequencies are not shifted, i.e., to each geometry at the A//A level there corresponds a set of original frequencies (calculated at the A//A level) and a shifted energy (calculated at the B//A level).

The potential energy curves for the three abstraction channels of the OH + glycolaldehyde reaction are very similar for both conformers. The hydroxyl abstraction potential curves are thinner and steeper than those corresponding to abstractions from $-CH_2$ and $-CHO$ groups. Accordingly, a larger tunneling effect should be expected for channels **Ic** and **IIc**. The behavior of V_a^G and E_{int} is also quite similar in shape to the one for a methyl hydrogen abstraction reaction by the Cl radical recently studied by Rosenman et al.[83] and to those of glyoxal and methylglyoxal + OH reactions.[77] Since V_a^G is obtained by summing V_{MEP} and E_{int}, the substantial drop in the E_{int} curve prior to the saddle point zone is responsible for the shape of the overall ground-state vibrationally adiabatic surface (V_a^G). The drop in the zero point energy, E_{int}, is not unique and it is characteristic of hydrogen abstraction reactions. Some examples can be found in refs 83−86. When this kind of profile is combined with a low and broad classical barrier, it causes a large shift of the variational transition state, i.e., there is a large variational effect (see ref 83 for more details). In these cases, the recrossing problem is essential, and variational transition state theory (VTST) theory is needed to obtain reliable values of the rate constants.

Rate Coefficients. According to the reaction mechanism proposed above, if k_1 and k_{-1} are the forward and reverse rate constants for the first step and k_2 corresponds to the second step, a steady-state analysis leads to a rate coefficient for the overall reaction channel which can be written as

$$k = \frac{k_1 k_2}{k_{-1} + k_2} \quad (14)$$

Even though the energy barrier for k_{-1} is about the same size as that for k_2, the entropy change is much larger in the reverse reaction than in the formation of the products. Thus, k_{-1} is expected to be considerably larger than k_2. On the basis of this assumption, first considered by Singleton and Cvetanovic,[87] k can be rewritten as

$$k = \frac{k_1 k_2}{k_{-1}} = K_{eq} k_2 \quad (15)$$

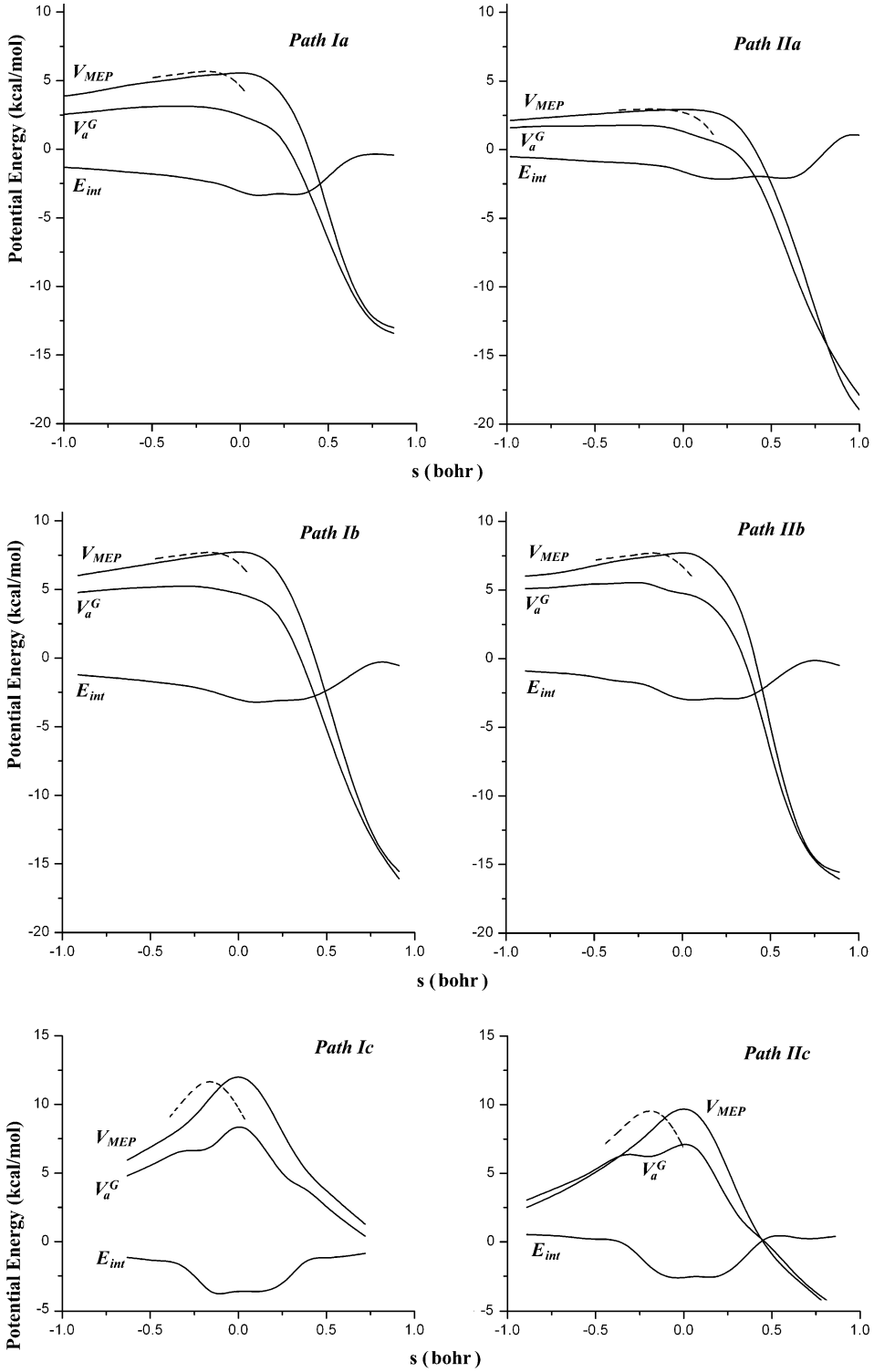

Figure 6. Classical potential energy paths (V_{MEP}) calculated at the CCSD(T) level, internal energies (E_{int}) calculated at the BHandHLYP level, and vibrationally adiabatic potential energy curves (V_a^G) as a function of the reaction coordinate, *s*. All energies are calculated relative to the corresponding reactant complexes.

where K_{eq} is the equilibrium constant between the isolated reactants and the reactant complex and k_2 is the rate constant corresponding to the second step of the mechanism, i.e., transformation of the reactant complex into products. In the absence of conclusive experimental data, we have assumed that the reactant complex undergoes collisional stabilization, that is, that the reaction occurs at the high pressure limit. This approach has been previously used to describe OH radical reactions with several volatile organic compounds (VOCs), including alkenes,[88] aldehydes,[89] alcohols,[90] formic acid,[91] and ketones.[92] It is also adequate to account for the experimental negative activation energy observed for the glycolaldehyde + OH reaction.

In a classical treatment, the influence of the complex exactly cancels in eq 8, and the overall rate coefficient depends only on the properties of OH, glycolaldehyde and the transition states. However, in the present case, there is a possibility of quantum mechanical tunneling, and the existence of the complex implies that several vibrational energy levels may be involved, with the corresponding increase in the tunneling factor, κ. We have assumed that a thermal equilibrium distribution of energy levels

TABLE 2: Energy Barriers (V_0), Frequencies (ν_i), Rotation Axis, and Internal Symmetry Number (σ_{int}) of the Motions That Have Been Considered as Internal Rotations

	V_0 (kcal/mol)	ν_i (cm^{-1})	axis	σ_{int}
conformer **I**	2.4	374.1	C1O4	2
TS−Ia	1.1	123.7	C2H7O9	2
TS−Ia	1.5	157.5	C1O4	2
TS−Ib	1.9	139.9	C1H5O9	1
TS−Ic	3.6	427.0	H8O9	1
TS−IIa	2.9	233.5	H7O9	1
TS−IIb	1.6	234.3	C1H5O9	1

is maintained, which corresponds to the high-pressure limiting behavior. Thus, all energy levels from the bottom of the well of the complex up to the barrier might contribute to tunneling. In the low-pressure limiting case, the lack of collisional stabilization means that none of the OH + glycolaldehyde entrance complexes can reach energies below reactants, and tunneling decreases considerably. The rate coefficient that is calculated using this approach presents a 75% discrepancy with the experimental value of k^{298}, compared to 30% when the high-pressure limit is considered. This difference supports our initial hypothesis.

We assume that neither mixing nor crossover between different pathways occurs and that the rate constant (k) corresponding to each conformer of glycolaldehyde + OH is determined as the sum of the rate coefficients of each path:[93]

$$k_{\mathrm{I}} = k_{\mathrm{Ia}} + k_{\mathrm{Ib}} + k_{\mathrm{Ic}} \tag{16}$$

$$k_{\mathrm{II}} = k_{\mathrm{IIa}} + k_{\mathrm{IIb}} + k_{\mathrm{IIc}} \tag{17}$$

To calculate the reaction path symmetry factor corresponding to each channel, we have used the following analysis. The symmetry point group for OH is $C_{\infty v}$ and for conformers **I** and **II** is C_s, all of them with symmetry numbers equal to 1,[94] leading to $\sigma^{\mathrm{R}} = 1$ for all the studied channels. The symmetry point group for all the transition states is C_1, also with symmetry number $\sigma^{\mathrm{GT}} = 1$. Therefore, for reaction paths **Ia**, **Ic**, **IIa**, and **IIc**, with $n = 1$ the reaction path symmetry number is 1 for the abstraction processes, which is intuitively reasonable since the OH can abstract only one H atom from the aldehydic and hydroxylic sites. Following the same reasoning for reaction paths **Ib** and **IIb**, σ^{R} and σ^{GT} are both equal to 1, but in these cases $n = 2$ since the transition states are chiral (Figure 3) and have optical isomers. Consequently, $\sigma(\mathbf{Ib}) = 2$ and $\sigma(\mathbf{IIb}) = 2$. This also agrees with our intuitive notion that there are two equivalent H atoms to be abstracted from the $-CH_2-$ site.

The frequencies, barriers, axis of rotation, and σ_{int} values corresponding to the vibrational modes that have been considered as internal rotations are reported in Table 2. They all correspond to the transition state structures. All the partition functions corresponding to the reactant complexes were calculated using the harmonic oscillator approximation. This saves computational time and introduces no error in the rate constant calculation since the partition functions corresponding to the RC cancel in eq 15, because of the $K_{eq}k_2$ product.

The overall rate coefficient, which measures the rate of OH disappearance, can be calculated at each temperature as

$$k_{\mathrm{overall}} = p_{\mathbf{I}}\, k_{\mathbf{I}} + p_{\mathbf{II}}\, k_{\mathbf{II}} \tag{18}$$

where $p_{\mathbf{I}}$ and $p_{\mathbf{II}}$ account for the fractions of conformers **I** and **II**, respectively. That this expression can be used is supported by the fact that interconversion is much less favored than H abstraction (Table 1).

TABLE 3: Rate Coefficients, in cm^3 $Molecule^{-1}$ s^{-1}, Branching Ratios (Γ), and Fractions of Conformers I and II, within the Temperature Range 200−500 K

T (K)	$k_{\mathbf{I}}$ ($\times 10^{12}$)	$k_{\mathbf{II}}$ ($\times 10^{12}$)	$p_{\mathbf{I}}$	$p_{\mathbf{II}}$	k_{overall} ($\times 10^{12}$)	$\Gamma_{\mathbf{a}}$	$\Gamma_{\mathbf{b}}$	$\Gamma_{\mathbf{c}}$
200	30.9	14.0	0.98	0.02	30.6	94.8	5.2	0.0
220	19.7	16.6	0.98	0.02	19.6	95.0	4.9	0.1
240	13.7	18.3	0.97	0.03	13.9	93.6	6.4	0.1
260	10.2	19.2	0.96	0.04	10.5	92.2	7.8	0.1
270	8.92	19.5	0.95	0.05	9.40	91.5	8.4	0.1
280	7.91	19.6	0.95	0.05	8.50	90.8	9.1	0.1
290	7.08	19.5	0.94	0.06	7.77	90.2	9.7	0.1
298.15	6.51	19.4	0.94	0.06	7.29	89.8	10.1	0.1
300	6.39	19.3	0.94	0.06	7.18	89.7	10.2	0.1
310	5.81	19.1	0.93	0.07	6.70	89.1	10.8	0.1
320	5.33	18.8	0.93	0.07	6.30	88.6	11.3	0.1
330	4.91	18.4	0.92	0.08	5.97	88.1	11.8	0.1
340	4.55	17.9	0.92	0.08	5.68	87.6	12.3	0.2
350	4.24	17.5	0.91	0.09	5.44	87.1	12.7	0.2
360	3.97	17.0	0.90	0.10	5.22	86.6	13.2	0.2
370	3.73	16.5	0.90	0.10	5.04	86.2	13.7	0.2
380	3.51	16.0	0.89	0.11	4.88	85.7	14.1	0.2
390	3.33	15.5	0.88	0.12	4.73	85.2	14.6	0.2
400	3.16	15.0	0.88	0.12	4.60	84.7	15.1	0.2
420	2.86	14.1	0.87	0.13	4.37	83.7	16.1	0.2
440	2.62	13.3	0.85	0.15	4.18	82.7	17.0	0.2
460	2.42	12.5	0.84	0.16	4.02	81.7	18.1	0.3
480	2.25	11.8	0.83	0.17	3.89	80.6	19.1	0.3
500	2.11	11.2	0.82	0.18	3.77	79.5	20.2	0.4

In eq 18, we are considering that cis and trans conformers of glycolaldehyde behave as different molecules. The corresponding rotational barriers are high enough to hinder the conformers interconversion. The cis → trans adiabatic barrier is equal to 5.4 kcal/mol and the trans → cis barrier is 3.0 kcal/mol at BHandHLYP/6-311++G(d,p) level of theory. Comparing them with values in Table 1, it can be seen that the adiabatic barriers of the main abstractions are lower than those of the interconversions. Accordingly, the conformers interconversion is much less favored than the H abstractions, thus the separation made in eq 18 is supported, especially for the main paths considered, i.e., the abstractions from −CHO and $-CH_2-$ groups.

The value of the overall rate coefficient, calculated using the CVT/SCT approach is reported in Table 3, together with $k_{\mathbf{I}}$, $k_{\mathbf{II}}$, and the fractions of both conformers.

Detail information on the equilibrium constants, the rate constants of the second step, tunneling corrections and the reaction coordinate of the variational transition states corresponding to all the studied paths are provided in Tables S1−S3, as Supporting Information. Tunneling corrections corresponding to abstractions from the OH group are appreciably larger than those corresponding to abstractions from the $-CH_2-$ and −CHO sites, for both conformers, as expected from the shape of the MEPs. For abstractions from the other two sites, tunneling is smaller but yet important enough to be taken into account. In addition, and for the whole temperature range between 200 and 500 K, the largest values of K_{eq} correspond to abstractions from the $-CH_2-$ sites, while the largest k_2 values correspond to abstractions from the −CHO sites. According to these results, k_2 plays a mayor role in the preponderance of −CHO abstractions over those from other sites. This finding together with the presence of tunneling, makes the inclusion of the reactant complex vital in order to reproduce the experimental data.

In Table 3, the branching ratios corresponding to abstraction from the −CHO (Γ*a*), $-CH_2$ (Γ*b*) and −OH (Γ*c*) sites have

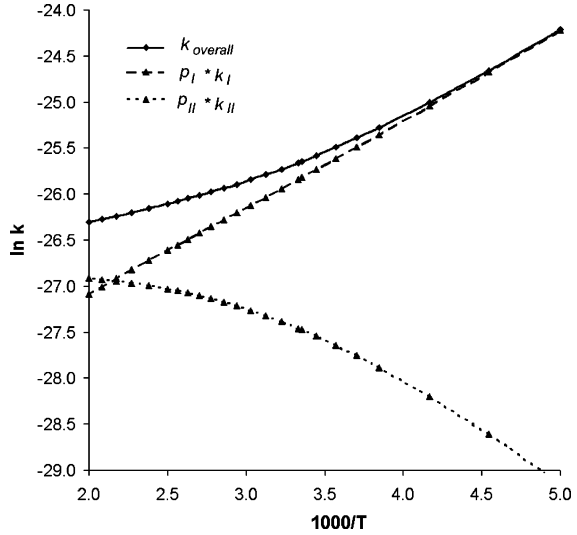

Figure 7. Arrhenius plots in the temperature range 200−500 K.

also been included. They have been calculated as

$$\Gamma_{\text{a, b, or c}} = \frac{k_{\text{a, b, or c}}}{k_{\text{overall}}} \times 100 \qquad (19)$$

There is good agreement between the experimental and calculated values of k_{overall}, at 298 K. Differences between our value and those reported by Niki et al.[14] and Bacher et al.[15] are 27% and 34%, respectively. There is also a good agreement between the branching ratios reported in ref 14 and the values calculated in this work. These coincidences support the validity of the proposed mechanism and of the level of theory used for both electronic and rate constant calculations. According to our results, as the temperature increases, the proportion of H abstraction from sites other than the aldehyde site increases slightly. However, abstraction from the −CHO group (paths a) remains dominant over the whole range of temperatures studied.

According to the results shown in Table 3, the contribution of the less stable conformer to the overall rate coefficient should be taken into account. Even though there is a very small population of the OO-*s*-trans conformer (**II**), the contribution of the term $p_{\mathbf{II}}k_{\mathbf{II}}$ to the overall rate coefficient is not negligible. Inclusion of this term is especially relevant as the temperature increases because its fraction becomes larger and the ratio $k_{\mathbf{II}}/k_{\mathbf{I}}$ also increases. Thus, neglecting this term would affect the values of the overall rate coefficient as well as the Arrhenius parameters: k_{overall} would decrease and the activation energy would become more negative. It would also lead to an artificially linear Arrhenius plot.

The variational transition states corresponding to paths **Ia**, **Ib**, **IIa**, and **IIb** are located on the reactants side, at *s* values equal to −0.4, −0.3, −0.6, and −0.3 bohr, respectively, for the whole temperature range (Tables S1−S3). The variational TS corresponding to path **Ic** is located on the products side, with $s = 0.01$ bohr. The variational **TS-IIc** is located on the products side at temperatures 200−310 K with $s = 0.1$ bohr, but it is on the reactants side at 320−500 K, with $s = -0.3$ bohr. Tunneling effects are found to be small but relevant for H abstractions from the −CHO and $-CH_2$ groups, and much larger for abstraction from the hydroxyl group, as expected according to the shape of the potential energy surfaces.

The influence of temperature on the rate of the chemical reactions studied in this work has been interpreted in terms of the Arrhenius equation[95]

$$k = A\mathrm{e}^{-E_a/RT} \qquad (20)$$

where *A* is known as the preexponential factor or the frequency factor, and E_a represents the activation energy. In eq 20 the influence of the temperature is accounted for in the exponential part of the expression. Since the Arrhenius equation is probably the most widely used today to interpret kinetic data, it is convenient to use it in the characterization of the rate constants, for later comparisons.

TABLE 4: Arrhenius and Kooij Parameters in the 280−320 and 200−500 K Temperature Ranges, Respectively

parameters	overall reaction
Arrhenius	
A (cm^3 molecule^{-1} s^{-1})	7.76×10^{-13}
E_a (kcal/mol)	−1.33
Kooij	
B (cm^3 molecule^{-1} s^{-1})	1.09×10^{-21}
m	3.03
E_0 (kcal/mol)	−3.19

As can be seen in Figure 7, the Arrhenius plots corresponding to k_{overall} and $k_{\mathbf{I}}$ are linear, while the plot corresponding to $k_{\mathbf{II}}$ is significantly curved. Consequently, E_a(**I**) does not change in the temperature range 200−500 K, while E_a(overall) and E_a(**II**) do. Since there are no unique values for E_a(overall) and E_a(**II**) in the studied temperature range, the Arrhenius equation does not properly describe the influence of temperature on the corresponding rate coefficients. However, the activation energy can be written as

$$\frac{\mathrm{d}(\ln k)}{\mathrm{d}T} \equiv \frac{E_a}{RT^2} \qquad (21)$$

which is equivalent to

$$\frac{\mathrm{d}(\ln k)}{\mathrm{d}(1/T)} \equiv -\frac{E_a}{R} \qquad (22)$$

Accordingly, when ln *k* is plotted against 1/*T*, the slope at any point is equal to $-E_a/R$, i.e., E_a can be calculated at any temperature from the slope of the tangent to the curve at the desired point, regardless of whether the Arrhenius plot is linear or not. We have calculated the Arrhenius activation energies in a rather small temperature range, around 298 K, where the curvature of the plots can be ignored. The chosen range was 280−320 K, and the corresponding Arrhenius parameters, calculated within the CVT/SCT approach, are shown in Table 4. A negative temperature dependence is obtained for the overall reaction, as expected based on the E_a values for the reactions of OH radicals with similar molecules such as propanal and methylglyoxal.[96] The proposed Arrhenius activation energy is −1.33 kcal/mol.

However, the procedure most commonly used to analyze the data when the plot of ln *k* vs 1/*T* is not linear is to use the equation proposed by Kooij:[97]

$$k = BT^m\mathrm{e}^{-E_0/RT} \qquad (23)$$

where *B*, E_0, and *m* are temperature independent parameters. This expression is more satisfactory than eq 13, from both the theoretical and empirical points of view. Even data that show significant deviations from the Arrhenius equation can usually be fitted very well by eq 23. Its applicability can be tested by

TABLE 5: Variation of the Activation Energies (kcal/mol) with Temperature (K), in the 200−500 K Range

T	E_a (overall)
200	−1.98
220	−1.86
240	−1.74
260	−1.62
270	−1.56
280	−1.50
290	−1.44
298.15	−1.39
300	−1.38
310	−1.32
320	−1.26
330	−1.20
340	−1.14
350	−1.08
360	−1.02
370	−0.96
380	−0.90
390	−0.84
400	−0.78
420	−0.66
440	−0.54
460	−0.42
480	−0.30
500	−0.18

plotting $\ln(k/T^m)$ vs $1/T$. If a straight line is obtained, its slope is equal to $-E_0/R$, and E_0 can be calculated. Differentiation of eq 23 in its logarithmic form leads to

$$\frac{d(\ln k)}{dT} = \frac{E_0 + mRT}{RT^2} \tag{24}$$

and comparing eqs 21 and 24, it is clear that the activation energy can be calculated, at each temperature, as

$$E_a = E_0 + mRT \tag{25}$$

where E_0 is the hypothetical activation energy at 0 K.

In our case, a plot of $\ln(k/T^m)$ vs $1/T$ yields a straight line, with R^2 equal to 0.9991, thus proving the applicability of the procedure that has been used to describe the influence of the temperature on the rate coefficient. The Kooij parameters that best fit the data are shown in Table 4. They were obtained by a nonlinear square analysis. Since the starting values are of great importance in such procedure, we have obtained them by following the suggestions in reference 98 for a similar function. We have performed a multiple regression analysis, taking ln *T* and $1/T$ as independent variables, since there is no multicollinearity among them, and ln *k* as the dependent variable. The results obtained for E_0, *m*, and *B* were then used as the starting values in the nonlinear square analysis, leading to the final figures reported in Table 4. Since none of the three parameters was fixed and the nonlinear analysis led to an R^2 coefficient of 0.9998, the procedure described here seems to be more reliable than those that use a fixed *m* (usually $m = 2$), which can lead to different E_0, *m*, and *B*, depending on the *m* value.

It could be interesting to discuss the variation of the activation energy with temperature (Table 5). The Kooij overall activation energy is negative in the whole range studied, and it increases as temperature rises. It goes from −1.98 kcal/mol at 200 K to −0.18 kcal/mol at 500 K. At 298 K, it is in excellent agreement with the one obtained using the Arrhenius approach: E_a(Arrhenius) = −1.33 kcal/mol and E_a(Kooij) = −1.39 kcal/mol. Accordingly, our predicted activation energy at 298 K can be given as −1.36 ± 0.03 kcal/mol, and the two and three parameters equations for the overall reaction are $k_{overall} = 7.760 \times 10^{-13} e^{1328/RT}$ cm^3 molecule^{-1} s^{-1} and $k_{overall} = 1.09 \times 10^{-21} T^{3.03} e^{3187/RT}$ cm^3 molecule^{-1} s^{-1}, respectively.

As mentioned above, Kwok and Atkinson[16] listed glycolaldehyde as one of the molecules for which the measured rate coefficient differs, by more than a factor of 2, from the one estimated using structure−activity relationships (SAR). The SAR approach is usually an excellent method to predict rate coefficients of atmospheric chemical reactions. However, it works best when there are no dynamic factors affecting the system's reactivity. The glycolaldehyde + OH rate constant that is predicted by SAR is 2.3×10^{-11} cm^3·molecule^{-1}·s^{-1}, while the experimental values are 1.0 and 1.1×10^{-11} cm^3 molecule^{-1} s^{-1}.[14,15] Since our calculated rate coefficient and our calculated branching ratios are in very good agreement with the experimental values, we have attempted to find an explanation for the discrepancy. For that purpose, the reaction profiles of the acetaldehyde and ethanol + OH reactions have been modeled using exactly the same methodology as for the glycolaldehyde + OH reaction. We found that the ZPE corrected barriers for H abstractions from the α position in ethanol and from the aldehydic site in acetaldehyde are 0.2 kcal/mol lower than the ones for the equivalent abstractions in glycolaldehyde. This difference is responsible for the decrease in *k*. In SAR, the deactivation of the $-CH_2$ site by the >C═O substituent is taken into account by introducing a factor $F(>C{=}O) = 0.75$. However, no deactivation is considered for the aldehydic abstraction. The deactivation occurs because of the intramolecular hydrogen bond in OO-*s*-*cis*-glycolaldehyde, which is a very specific characteristic of this molecule.

According to SAR, the presence of an oxygen atom increases the rate coefficient of the aldehydic hydrogen by a factor of 8.7, as compared to the −CH< group in alkanes. This effect is reduced by the intramolecular hydrogen bond because the H in the OH group is competing for the unpaired electrons of the carbonyl group in the transition state. For this reason the intramolecular hydrogen bond in the TS is longer, by 0.16 Å, compared to free glycolaldehyde. A different situation occurs in the abstraction from the $-CH_2$ group. The presence of the OH group increases the rate coefficient (k_{CH_2}) by a factor of 3.5 (2,9),[16] while the presence of the >C═O group reduces it by a factor of 0.75, as compared to $-CH_2$ in alkanes. In this case the change in the intramolecular hydrogen bond distance in the TS is insignificant, according to our calculations, suggesting that the intramolecular hydrogen bond does not affect H abstraction from this site. The proposed experimental k_{CH_2} is 2.0×10^{-12}, in excellent agreement with the SAR prediction of 2.45 (2.03) $\times 10^{-12}$ cm^3 molecule^{-1} s^{-1}.

In addition, the calculated rate coefficient for the OO-*s*-trans-glycolaldehyde is 1.94×10^{-11}, which is in excellent agreement with the SAR prediction of 2.03×10^{-11}. This finding also supports the idea that the intramolecular hydrogen bond is responsible for the discrepancies between SAR and experimental results. Therefore, the SAR approach accurately predicts the rate coefficient of the OH reaction with conformer **II**, as well as the $-CH_2-$ partial rate.

Another theoretical study on glycolaldehyde + OH system has been published while this work was in preparation.[99] It was not cited in more detail, since we became aware of this publication thanks to a Reviewer of the present work.

Conclusions

The OH abstraction reaction from glycolaldehyde has been modeled according to a complex mechanism involving the

formation of a reactant complex in the entrance channel and of a product complex in the exit channel. Two conformers have been considered in the modeling and, for each of them, H abstractions from three possible sites have been computed: (a) −CHO, (b) $-CH_2$, and (c) −OH.

The MEP was computed using the two-level theory approach known as B//A, which consists of a geometry optimization at level A, followed by a single point calculation at a higher level B. The chosen levels were A = BHandHLYP/6-311++G-(d,p) and B = CCSD(T)/6-311++G(d,p). The vibrationally adiabatic potential energy surface is low and broad, supporting the use of the CVT/SCT approach to calculate the rate coefficients.

The abstraction from the aldehydic site was found to be dominant within the whole temperature range, varying from 95% at 200 K to 80% at 500 K. At 298 K, its contribution to the overall reaction was found to be 89.8%. The calculated overall rate coefficient ($k_{overall}$) was found to be equal to 7.29×10^{-12} cm^3 $molecule^{-1}$ s^{-1}. Both $k_{overall}$ and the branching ratios are in very good agreement with the experimental findings previously reported at 298 K.

The temperature dependence of the overall rate coefficient is best fitted by the expressions $k_{overall} = 7.76 \times 10^{-13} e^{1328/RT}$ cm^3 $molecule^{-1}$ s^{-1} and $k_{overall} = 1.09 \times 10^{-21} T^{3.03} e^{3187/RT}$ cm^3 $molecule^{-1}$ s^{-1}, corresponding to the Arrhenius and Kooij approaches, respectively. The predicted activation energy is (−1.36 ± 0.03) kcal/mol, around 298 K.

The intramolecular hydrogen bond in OO-*s*-cis glycolaldehyde was found to be responsible for the discrepancies between SAR and experimental rate coefficients.

Acknowledgment. The authors gratefully acknowledge the financial support from the Instituto Mexicano del Petróleo (IMP) through program D00179. We also thank the IMP Computing Center for supercomputer time on SGI Origin 3000. We thank Professors S. Zhang and T. N. Truong for providing access to the cseo.net site through the Internet.[48]

Supporting Information Available: Tables S1−S3, giving equilibrium constants (K_{eq}, cm^3 $molecule^{-1}$ s^{-1}), rate constants of the second step, (k_2, s^{-1}), tunneling corrections (κ), and reaction coordinate (*s*, bohr) of the variational transition state, corresponding to the abstractions from the −CHO, −OH, and $-CH_2$ sites. This material is available free of charge via the Internet at http://pubs.acs.org.

References and Notes

(1) Mason, S. A.; Field, R. J.; Yokelson, R. J.; Kochivar, M. A.; Tinsley, M. R.; Ward, D. E.; Hao, W. M. *J. Geophys. Res.-Atmos.* **2001**, *106*, 12527.

(2) Goode, J. G.; Yokelson, R. J.; Susto, R. A.; Ward, D. E. *J. Geophys. Res.-Atmos.* **1999**, *104*, 21237.

(3) Christian, T. J.; Kleiss, B.; Yokelson, R. J.; Holzinger, R.; Crutzen, P. J.; Hao, W. M.; Shirai, T.; Blake, D. R. *J. Geophys. Res.-Atmos.* **2004**, *109*, 2311.

(4) Christian, T. J.; Kleiss, B.; Yokelson, R. J.; Holzinger, R.; Crutzen, P. J.; Hao, W. M.; Saharjo, B. H.; Ward, D. E. *J. Geophys. Res.-Atmos.* **2003**, *108*, 4719.

(5) Bertschi, I.; Yokelson, R. J.; Ward, D. E.; Babbitt, R. E.; Susott, R. A.; Goode, J. G.; Hao, W. M. *J. Geophys. Res.-Atmos.* **2003**, *108*, 8472.

(6) Noda, J.; Hallquist, M.; Langer, S.; Ljungstrom, E. *Phys. Chem. Chem. Phys.* **2000**, *2*, 2555.

(7) Alvarado, A.; Tuazon, E. C.; Aschmann, S. M.; Arey, J.; Atkinson, R. *Atmos. Environ.* **1999**, *33*, 2893.

(8) Ferronato, C.; Orlando, J. J.; Tyndall, G. S. *J. Geophys. Res.-Atmos.* **1998**, *103*, 25579.

(9) Grosjean, E.; Grosjean, D. *J. Atmos. Chem.* **1999**, *32*, 205.

(10) Orlando, J. J.; Tyndall, G. S.; Ceazan, N. *J. Phys. Chem.* A. **2001**, *105*, 3564.

(11) Fantechi, G.; Jensen, N. R.; Hjorth, J.; Peeters, J. *Atmos. Environ.* **1998**, *32*, 3547.

(12) Atkinson, R.; Tuazon, E. C.; Aschmann, S. M. *Int. J. Chem. Kinet.* **1998**, *30*, 577.

(13) Orlando, J. J.; Tyndall, G. S. *J. Phys. Chem.* A. **2002**, *106*, 12252.

(14) Niki, H.; Maker, P. D.; Savage, C. M.; Hurley, M. D. *J. Phys. Chem.* **1987**, *91*, 2174.

(15) Bacher, C.; Tyndall, G. S.; Orlando, J. J. *J. Atmos. Chem.* **2001**, *39*, 171.

(16) Kwok, E. S. C.; Atkinson, R. *Atmos. Environ.* **1995**, *29*, 1685.

(17) Niki, H.; Maker, P. D.; Savage, C. M.; Breitenback, L. P. *J. Phys. Chem.* **1984**, *88*, 5342.

(18) Temps, F.; Wagner, H. Gg. *Ber. Bunsen-Ges. Phys. Chem.* **1984**, *88*, 415.

(19) D'Anna, B.; Langer, S.; Ljungström, E.; Nielsen, C. J.; Ullerstam, M. *Phys. Chem. Chem. Phys.* **2001**, *3*, 1631.

(20) Vandenberk, S.; Peeters, J. *J. Photochem. Photobiol. A-Chem.* **2003**, *157*, 269.

(21) Dupuis, M.; Lester, W. A., Jr. *J. Chem. Phys.* **1984**, *81*, 847.

(22) Soto, M. R.; Page, M. *J. Phys. Chem.* **1990**, *94*, 3246.

(23) Francisco, J. S. *J. Chem. Phys.* **1992**, *96*, 7597.

(24) Alvarez-Idaboy, J. R.; Mora-Diez, N.; Boyd, R. J.; Vivier-Bunge, A. *J. Am. Chem. Soc.* **2001**, *123*, 2018.

(25) Aloisio, S.; Francisco, J. S. *J. Phys. Chem. A* **2000**, *104*, 3211.

(26) Vasvári, V.; Szilágyi, I.; Bencsura, A.; Dóbe, S.; Berces, T.; Henon, E.; Canneaux, S.; Bohr, F. *Phys. Chem. Chem. Phys.* **2001**, *3*, 551.

(27) Galano, A.; Alvarez-Idaboy, J. R.; Bravo-Perez, G.; Ruiz-Santoyo, Ma. E. *Phys. Chem. Chem. Phys.* **2002**, *4*, 4648.

(28) Galano, A.; Alvarez-Idaboy, J. R.; Ruiz-Santoyo, Ma. E.; Vivier-Bunge, A. *J. Phys. Chem. A* **2002**, *106*, 9520.

(29) Henon, E.; Canneaux, S.; Bohra, F.; Dóbe, S. *Phys. Chem. Chem. Phys.* **2003**, *5*, 333.

(30) Yamada, T.; Taylor, P. H.; Goumri, A.; Marshall, P. *J. Chem. Phys.* **2003**, *119*, 10600.

(31) Smith, I. W. M.; Ravishankara, A. R. *J. Phys. Chem. A* **2002**, *106*, 4798.

(32) Loomis, R. A.; Lester, M. I. *J. Chem. Phys.* **1995**, *103*, 4371.

(33) Lester, M. I.; Pond, B. V.; Anderson, D. T.; Harding, L. B.; Wagner, A. F. *J. Chem. Phys.* **2000**, *113*, 9889.

(34) Tyndall, G. S.; Orlando, J. J.; Wallington, T. J.; Hurley, M. D. *Phys. Chem. Chem. Phys.* **2002**, *4*, 2189.

(35) Gaussian 98, Revision A.3. Frisch, M. J.; Trucks, G. W.; Schlegel, H. B.; Scuseria, G. E.; Robb, M. A.; Cheeseman, J. R.; Zakrzewski, V. G.; Montgomery, J. A., Jr.; Stratmann, R. E.; Burant, J. C.; Dapprich, S.; Millam, J. M.; Daniels, A. D.; Kudin, K. N.; Strain, M. C.; Farkas, O.; Tomasi, J.; Barone, V.; Cossi, M.; Cammi, R.; Mennucci, B.; Pomelli, C.; Adamo, C.; Clifford, S.; Ochterski, J.; Petersson, G. A.; Ayala, P. Y.; Cui, Q.; Morokuma, K.; Malick, D. K.; Rabuck, A. D.; Raghavachari, K.; Foresman, J. B.; Cioslowski, J.; Ortiz, J. V.; Stefanov, B. B.; Liu, G.; Liashenko, A.; Piskorz, P.; Komaromi, I.; Gomperts, R.; Martin, R. L.; Fox, D. J.; Keith, T.; Al-Laham, M. A.; Peng, C. Y.; Nanayakkara, A.; Gonzalez, C.; Challacombe, M.; Gill, P. M. W.; Johnson, B.; Chen, W.; Wong, M. W.; Andres, J. L.; Gonzalez, C.; Head-Gordon, M.; Replogle, E. S.; Pople, J. A. Gaussian Inc.: Pittsburgh, PA, 1998.

(36) Becke, A. D. *J. Chem. Phys.* **1993**, *98*, 1372.

(37) Raghavachari, K.; Foresman, J. B.; Cioslowski, J.; Ortiz, J. V.; Frisch, M. J.; Frisch, A. *GAUSSIAN 98 User's Reference*; Gaussian Inc.: Pittsburgh, PA, 1998.

(38) Keck, J. C. *J. Chem. Phys.* **1960**, *32*, 1035.

(39) Baldridge, K. M.; Gordon, M. S.; Steckler, R.; Truhlar, D. G. *J. Phys. Chem.* **1989**, *93*, 5107.

(40) Garrett, B. C.; Truhlar, D. G.; Grev, R. S.; Magnuson, A. W. *J. Phys. Chem.* **1980**, *84*, 1730. Erratum: **1983**, *87*, 4554.

(41) Isaacson, A. D.; Truhlar, D. G. *J. Chem. Phys.* **1982**, *76*, 1380.

(42) Truhlar, D. G.; Isaacson, A. D.; Garrett, B. C. In *Theory of Chemical Reaction Dynamics*; Baer, M., Ed.; CRC Press: Boca Raton, FL, 1985; Vol. 4, pp 65−137.

(43) Truhlar, D. G.; Garrett, B. C. *Annu. Rev. Phys. Chem.* **1984**, *35*, 159.

(44) Lu, D.-h.; Truong, T. N.; Melissas, V.; Lynch, G. C.; Liu, Y.-P.; Garrett, B. C.; Steckler, R.; Isaacson, A. D.; Rai, S. N.; Hancock, G. C.; Lauderdale, J. G.; Joseph, T.; Truhlar, D. G. *Comput. Phys. Commun.* **1992**, *71*, 235.

(45) Truhlar, D. G.; Gordon, M. S. *Science* **1990**, *249*, 491.

(46) Truong, T. N.; Lu, D.-h.; Lynch, G. C.; Liu, Y.-P.; Melissas, V. S.; Stewart, J. J. P.; Steckler, R.; Garrett, B. C.; Isaacson, A. D.; Gonzalez-Lafont, A.; Rai, S. N.; Hancock, G. C.; Joseph, T.; Truhlar, D. G. *Comput. Phys. Commun.* **1993**, *75*, 143.

(47) Liu, Y.-P.; Lynch, G. C.; Truong, T. N.; Lu, D.-h.; Truhlar, D. G.; Garrett, B. C. *J. Am. Chem. Phys.* **1993**, *115*, 2408.

(48) Zhang, S.; Truong, T. N. Kinetics (CSEO version 1.0), University of Utah, **2003.**

(49) Truhlar, D. G.; Kupperman, A. *J. Am. Chem. Soc.* **1971**, *93*, 1840.

(50) Fukui, K. *Pure Appl. Chem.* **1982**, *54*, 1825.
(51) Fukui, K. *J. Phys. Chem.* **1970**, *74*, 4161.
(52) Gonzalez, C.; Schlegel, H. B. *J. Phys. Chem.* **1990**, *94*, 5523.
(53) Truhlar, D. G. Kupperman, A. *J. Am. Chem. Soc.* **1971**, *93*, 1840.
(54) Truhlar, D. G.; Isaacson, A. D.; Garrett, B. C. In *Theory of Chemical Reaction Dynamics*; Baer, M., Ed.; CRC Press: Boca Raton, 1985; Vol. 4, p 65.
(55) Eyring, H. *J. Chem. Phys.* **1935**, *3*, 107.
(56) Truhlar, D. G.; Hase, W. L.; Hynes, J. T. *J. Phys. Chem.* **1983**, *87*, 2664.
(57) Truhlar, D. G.; Garrett, B. C. *Acc. Chem. Res.* **1980**, *13*, 440.
(58) Truhlar, D. G.; Garrett, B. C. *Annu. Rep. Phys. Chem.* **1984**, *35*, 159.
(59) Truhlar, D. G.; Isaacson, A. D.; Garrett, B. C. In *Generalized transition state theory*; Truhlar, D. G., Isaacson, A. D., Garrett, B. C., Eds.; CRC Press: Boca Raton, FL, 1985; Vol. 4, p 65.
(60) Garrett, B. C.; Truhlar; D. G. *J. Phys. Chem.* **1979**, *83*, 1052.
(61) Garrett, B. C.; Truhlar; D. G. *J. Phys. Chem.* **1979**, *83*, 1079.
(62) Garrett, B. C.; Truhlar; D. G. *J. Am. Chem. Soc.* **1979**, *101*, 4534.
(63) Garrett, B. C.; Truhlar; D. G. *J. Phys. Chem.* **1979**, *83*, 3058.
(64) Schenter, G. K.; Garrett, B. C.; Truhlar, D. G. *J. Chem. Phys.* **2003**, *119*, 5828.
(65) Jacox, M. E. *Vibrational and Electronic Energy Levels of Polyatomic Transient Molecules*; NIST: Gaithersburg, MD, 1998: Vol. 69, p 945.
(66) Ayala, P. Y.; Schlegel, H. B. *J. Chem. Phys.* **1998**, *108*, 2314.
(67) (a) Pechukas, P. *J. Chem. Phys.* **1976**, *64*, 1516. (b) Pechukas, P. *Dinamics of Molecular Collisions, Part B*; Miller, W. H., Ed.; Plenum Press: New York, 1976. (c) Pollak, E.; Pechukas, P. *J. Am. Chem. Soc.* **1978**, *100*, 2984. (d) Gilbert, R. G.; Smith, S. C. *Theory of Unimolecular and Recombination Reactions*; Blackwell Scientific Publications: Oxford, U.K., 1990.
(68) Marcus, R. A.; Coltrin, M. E. *J. Chem. Phys.* **1977**, *67*, 2609.
(69) Lu, D.-h.; Truong, T. N.; Melissas, V. S.; Lynch, G. C.; Liu, Y.-P.; Garrett, B. C.; Steckler, R.; Isaacson, A. D.; Rai, S. N.; Hancock, G. C.; Lauderdale, J. G.; Joseph, T.; Truhlar, D. G. *Comput. Phys. Commun.* **1992**, *71*, 235.
(70) Liu, Y.-P.; Lynch, G. C.; Truong, T. N.; Lu, D.-h.; Truhlar, D. G.; Garrett, B. C. *J. Am. Chem. Soc.* **1993**, *115*, 2408.
(71) Liu, J.; Li, Z.; Dai, Z.; Huang, X.; Sun, C. *J. Phys. Chem. A.* **2001**, *105*, 7707.
(72) Masgrau, L.; Gonzalez-Lafont, A.; Lluch, J. M. *J. Phys. Chem. A.* **2002**, *106*, 11760.
(73) Espinosa-Garcia, J. *J. Phys. Chem. A.* **2002**, *106*, 5686.
(74) Liu, J.; Li, Z.; Dai, Z.; Huang, X.; Sun, C. *J. Phys. Chem. A.* **2003**, *107*, 6231.
(75) Espinosa-Garcia, J. *J. Phys. Chem. A.* **2003**, *107*, 1618.
(76) Masgrau, L.; Gonzalez-Lafont, A.; Lluch, J. M. *J. Phys. Chem. A.* **2003**, *107*, 4490.
(77) Galano, A.; Alvarez-Idaboy, J. R.; Ruiz-Santoyo, Ma. E.; Vivier-Bunge, A. *ChemPhysChem.* **2004**, *5*, 1379.
(78) Ratajczyk, T.; Pecul, M. Sadlej, J. *J. Phys. Chem. A* **2004**, *108*, 2758.
(79) Senent, M. L. *J. Phys. Chem. A* **2004**, *108*, 6286.
(80) Bader, R. F. W. *Atoms in Molecules−A Quantum Theory*, Oxford University Press: Oxford, U.K. 1990.
(81) Duncan, W. T.; Bell, R. L.; Truong, T. N. *J. Comput. Chem.* **1998**, *19*, 1039.
(82) Espinosa-Garcia, J.; Corchado, J. C. *J. Phys. Chem.* **1995**, *99*, 8613.
(83) Rosenman, E.; McKee, M. L. *J. Am. Chem. Soc.* **1997**, *119*, 9033.
(84) Corchado, J. C.; Espinosa-Garcia, J. *J. Chem. Phys.* **1997**, *106*, 4013.
(85) Natanson, G. A. *Chem. Phys. Lett.* **1992**, *190*, 209.
(86) Espinosa-Garcia, J.; Corchado, J. C. *J. Chem. Phys.* **1994**, *101*, 1333.
(87) Singleton, D. L.; Cvetanovic, R. J. *J. Am. Chem. Soc.* **1976**, *98*, 6812.
(88) Alvarez-Idaboy, J. R.; Mora-Diez, N.; Vivier-Bunge, A. *J. Am. Chem. Soc.* **2000**, *122*, 3715.
(89) Alvarez-Idaboy, J. R.; Mora-Diez, N.; Boyd, R. J.; Vivier-Bunge, A. *J. Am. Chem. Soc.* **2001**, *123*, 2018.
(90) Galano, A.; Alvarez-Idaboy, J. R.; Bravo-Perez, G.; Ruiz-Santoyo, M. E. *Phys. Chem. Chem. Phys.* **2002**, *4*, 4648.
(91) Galano, A.; Alvarez-Idaboy, J. R.; Ruiz-Santoyo, M. E.; Vivier-Bunge, A. *J. Phys. Chem. A* **2002**, *106*, 9520.
(92) Alvarez-Idaboy, J. R.; Cruz-Torres, A.; Galano, A.; Ruiz-Santoyo, M. E. *J. Phys. Chem. A* **2004**, *108*, 2740.
(93) Robinson, P. J.; Holbrook, K. A. *Unimolecular Reactions*; Wiley-Interscience: London, 1972.
(94) Irikura, K. K. *ACS Symp. Ser.* **1998**, *677*, 402.
(95) Arrhenius, S. *Z. Phys. Chem.* **1889**, *4*, 226.
(96) Atkinson, R.; Baulch, D. L.; Cox, R. A.; Hampson, R. F.; Kerr, J. A.; Rossi, M. J.; Troe, J. *J. Phys. Chem. Ref. Data* **2000**, *29*, 167.
(97) Kooij, D. M. *Z. Phys. Chem.* **1893**, *12*, 155.
(98) Draper, N. R.; Smith, H. *Applied Regression Analysis*; John Wiley & Sons: New York, 1966; Chapter 10, p 458.
(99) Ochando-Pardo, M.; Nebot-Gil, I.; Gonzalez-Lafont, A.; Lluch, J. M. *J. Phys. Chem. A* **2004**, *108*, 5117.